Information Technology Journal 11 (12): 1705-1713, 2012
ISSN 1812-5638 / DOI: 10.3923/itj.2012.1705.1713

Numerical Investigation on the Drag and Heat Flux Reduction of a Supersonic Reentry Capsule with a Counter-flow Jet

Chao-Ying Zhou, Wen-Ying Ji and Peng Xie
Shenzhen Graduate School, Harbin Institute of Technology Shenzhen Graduate School,
Shenzhen 518055, People's Republic of China

Abstract: The mixing flow field around a reentry capsule with a counter-flow jet from its front stagnation point in supersonic flow is numerically studied by solving the axisymmetric Navier-Stokes equation coupled with k-ε turbulence model using the Van Leer's flux vector splitting spatial discretion scheme. With the jet Mach number and total temperature fixed, the effects of jet total-pressure ratio on the flow structure, drag and heat flux on the body are investigated. The results show that two classical flow modes exist in the mixing flow field, one is long penetration mode and the other is short penetration mode. The drag on the blunt body is reduced significantly because of counter-flow jet. Considering the exhaustion of jet thrust, the effect of drag reduction is better when flow is in LPM than in SPM. It is found that the maximum drag reduction can reach as high as 55.8% for the cases studied. Blunt body heat flux can also be reduced significantly and can even be negative when jet total pressure ratio is high enough. The results may have some significance for the engineering application of supersonic blunt body counter-flow jet technology.

Key words: Reentry capsule, supersonic flow, counter-flow jet, drag reduction, heat flux reduction

INTRODUCTION

High shock wave drag and heavy aero-thermal loads are the two major problems encountered in supersonic and hypersonic vehicle aerodynamic design. The counter-flow jet as a active flow control technology to reduce wave drag and heat transfer has induced a considerable interest. It has a wide range of applications both in military and civilian and because of its physical complexity involving bow shock, contact surface of main flow and opposing jet, Mach disk, recirculation region and reattachment shock wave, make research on it is of great significance both in theory and applications (Warren, 1960; Meyer *et al*., 2001; Daso *et al*., 2009).

Various authors have suggested that the pressure and temperature distributions might be modified with advantage by the introduction of a secondary flow at the front stagnation point of the body and make widely investigation (Warren, 1960; Ganiev *et al*., 2000; Shang *et al*., 2002; Fomin *et al*., 2001). Romeo and Sterrett (1963) experiments shown that the main shock of blunt cones can be affected by the forward facing jet at the stagnation point in two significantly different ways. One way is to cause a large displacement of the main shock and considerably change its shape, the other is only to move the bow shock away from the body with altering its shape. Finley (1966) make a series of experimental investigations on the counter-flow jet at the stagnation point of a sphere cylinder in supersonic wind tunnel under different Mach number and jet exit size. The results shown that the drag on the blunt body was reduced because a part of the jet stream entrained to form a low pressure recirculation zone, there exist steady and unsteady flow mode and a sufficient condition for steady flow is developed.

Formin *et al*. (2002) made a side by side experiments and numerical simulations on the flow-field of nitrogen opposing jet heated by arc discharge on the fore-body of truncated cone cylinder models in Mach 2, 2.5 and 4 supersonic free-streams. The results revealed unsteady Long Penetration Mode (LPM) and steady Short Penetration Mode (SPM), with LPM jet giving larger drag reduction and shock stand-off distance.

Experimental measurements of Venukumar *et al*. (2006) shown about 30-45% reduction in drag coefficient for different jet pressure by supersonic jet for a large angle blunt cone at hypersonic Mach number. Meyer *et al*. (2001) made a numerical investigation on the effect of upstream injection on the wave drag, heat transfer and skin-friction drag of a spherical body. Among the condition tested wave drag including the drag penalty of the forward-facing jet is shown to be reduced by as

Corresponding Author: Wen-Ying Ji, Shenzhen Graduate School, Harbin Institute of Technology Shenzhen Graduate School, Shenzhen 518055, People's Republic of China

much as 55% and the heat-transfer rates was also found to be dramatically reduced. However, he only related this drag and heat flux reduction with shock stand-off distance and didn't connect them with the important phenomenon of flow mode transition. Shang *et al.* (2001) made a side-by-side experimental and computational investigation on the flow field and drag reduction effect of a counter flow from a hemispherical cylinder. When the control parameter of the stagnation pressure ratio between the oncoming stream and the counter-flow jet exceeds a critical value, there is a sudden change of the dynamic state from an oscillatory to nearly steady motion referred as jet bifurcation. The drag reduction reached at a maximum at the bifurcation point as high as 40%. Beyond the bifurcation point, the measured drag force first rise sharply and then sustains a continuous drop. Nair *et al.* (2010) established the effect of film cooling due to opposed jet on a blunted cone-flare in hypersonic flow. He concluded that the formation of a separation boundary layer of cold jet protects the surface of the module from aerodynamic heating.

The turbulence effect in this high speed flow is also attracted the attention of researchers. Shang *et al.* (2001) made laminal and turbulent numerical and experiment simulations on the counter-flow jet flow field and found that experimental observations didn't validate the flow structures of the laminal computation. This was also supported by the experimental finding of Debieve *et al.* (2003). Chen *et al.* (2011) numerical simulated the opposing jet in supersonic flow by using large eddy simulation method for two pressure ratios of the jet to the free-stream. The shock/turbulent interaction and turbulent shear layer evolution are systematically studied. All These investigations indicate that turbulent simulations are needed for correctly predict the shock and jet interaction flow field.

In this study, a numerical investigation on the possible effect of the counter-flow jet technology to reduce the shock wave drag and heat flux of a supersonic reentry capsule is taken. Through the detailed flow field description and the pressure and heat flux distribution on the model to make a better understanding of the flow physics and provide some vital information to push the technology readiness of counter-flow jet as a active flow control method to improve aerodynamic performance.

Physical model and numerical methods

Physical model: A two-dimensional axisymmetric 2.6%-scale Apollo capsule model with zero angle of attack is used in this study. The model geometry is shown in Fig. 1. The same as used by Daso *et al.* (2009). The forebody of the vehicle is a spherical cap with radius of

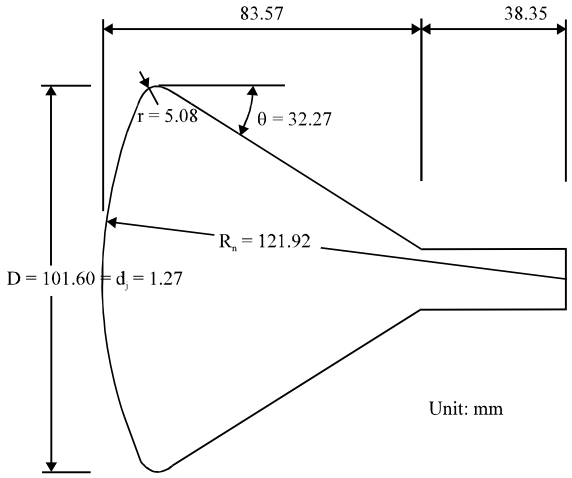

Fig. 1: Computation model

curvature and base radius of R_n = 121.92 mm and R = 50.8 mm, respectively. The shoulder radius is 5% of the base radius or 5.08 mm. The inverted cone angle is 32.27 degree. The jet nozzle exit is positioned at the stagnation point of the model with a diameter of 1.27 mm. $p_{0\infty}$, $T_{0\infty}$, M_∞, ε_∞ are the total pressure, total temperature, Mach number and specific-heat ratio of the free stream, respectively. Similarly, p_{0j}, T_{0j}, M_j, ε_j are the corresponding values of the jet. It remains to specify the jet total-pressure ratio P, given by $P = p_{0j}/p_{0f}$ where p_{0f} is the Pitot pressure of the free stream, the total pressure after a normal shock.

Governing equations and boundary condition: The Navier-Stokes equations were transformed to non-dimensional form by choosing the base diameter D, the free stream velocity U_∞, density ρ_∞ and viscosity efficient μ_∞ as the reference variable. The unsteady, two-dimensional, compressible, mass-averaged Navier-Stokes equations were written in the following strong-conservation form:

$$\frac{\partial Q}{\partial t}+\frac{\partial E}{\partial \xi}+\frac{\partial F}{\partial \eta}=\frac{1}{Re}\left(\frac{\partial E_v}{\partial \xi}+\frac{\partial F_v}{\partial \eta}\right)+S \quad (1)$$

where, t is the time, ξ, η the surface fitted computational coordinates, $Re = \rho_\infty U_\infty D/\mu_\infty$, Q the vector of dependent variables, E, F the non-viscous convective fluxes, E_v, F_v are the viscous diffusive fluxes and S the vector source term. The turbulence effects were accounted by incorporating standard k-ε model, where turbulent kinetic energy k and dissipation ε are defined by Launder and Spalding (1974).

With this formulation, the vector of dependent variables is given as:

$$Q=\begin{bmatrix}\rho\\ \rho u\\ \rho v\\ E_t\\ \rho k\\ \rho\varepsilon\end{bmatrix}\quad E=\frac{1}{J}\begin{bmatrix}\rho u\\ \rho uU+\xi_x p\\ \rho vU+\xi_y p\\ E_t U+\xi_{x_i}u_i p\\ \rho kU\\ \rho\varepsilon U\end{bmatrix}\quad F=\frac{1}{J}\begin{bmatrix}\rho V\\ \rho uV+\eta_x p\\ \rho vV+\eta_y p\\ E_t V+\eta_{x_i}u_i p\\ \rho kV\\ \rho\varepsilon V\end{bmatrix}$$

$$E_v=\frac{1}{J}\begin{bmatrix}0\\ \xi_{x_i}\tau_{i1}\\ \xi_{x_i}\tau_{i2}\\ \xi_{x_i}(u_j\tau_{ij}-q_i)\\ (\mu+\mu_t/\sigma_k)\xi_{x_i}\dfrac{\partial\xi_j}{\partial x_i}\dfrac{\partial k}{\partial\xi_j}\\ (\mu+\mu_t/\sigma_\varepsilon)\xi_{x_i}\dfrac{\partial\xi_j}{\partial x_i}\dfrac{\partial\varepsilon}{\partial\xi_j}\end{bmatrix}\quad F_v=\frac{1}{J}\begin{bmatrix}0\\ \eta_{x_i}\tau_{i1}\\ \eta_{x_i}\tau_{i2}\\ \eta_{x_i}(u_j\tau_{ij}-q_i)\\ (\mu+\mu_t/\sigma_k)\eta_{x_i}\dfrac{\partial\xi_j}{\partial x_i}\dfrac{\partial k}{\partial\xi_j}\\ (\mu+\mu_t/\sigma_\varepsilon)\eta_{x_i}\dfrac{\partial\xi_j}{\partial x_i}\dfrac{\partial\varepsilon}{\partial\xi_j}\end{bmatrix}$$

While the source term is:

$$S=\frac{1}{J}\begin{bmatrix}0\\ 0\\ 0\\ 0\\ P_k-\rho\varepsilon\\ C_{\varepsilon1}P_k\dfrac{\varepsilon}{k}-C_{\varepsilon2}\dfrac{\varepsilon^2}{k}\end{bmatrix}$$

Where:

$$U=\xi_t+\xi_{x_i}u_i$$

$$V=\eta_t+\eta_{x_i}u_i$$

$$E=\frac{p}{(\gamma-1)}+\frac{1}{2}\rho(u^2+v^2)$$

where, u, v, w are the Cartesian velocity components, p is the pressure, ρ is density and γ is specific heat ratio. The dependent variables of t, p, k , ε have been have been non-dimensionalized by D/U_∞, $\rho^2 U^2 {}_\infty U^2 {}_\infty$ and U^3/D_∞ respectively. Components of the heat flux vector and stress tensor may be expressed as:

$$q_i=-\left[\frac{1}{(\gamma-1)M_\infty^2}\right]\left(\frac{\mu}{Pr}+\frac{\mu_t}{Pr_t}\right)\frac{\partial\xi_j}{\partial x_i}\frac{\partial T}{\partial\xi_j}$$

$$\tau_{ij}=(\mu+\mu_t)\left(\frac{\partial\xi_k}{\partial x_j}\frac{\partial u_i}{\partial\xi_k}+\frac{\partial\xi_k}{\partial x_i}\frac{\partial u_j}{\partial\xi_k}-\frac{2}{3}\delta_{ij}\frac{\partial\xi_l}{\partial x_k}\frac{\partial u_k}{\partial\xi_l}\right)$$

The turbulence production item Pk is defined as:

$$P_k=\frac{1}{Re}\tau_{ij}\frac{\partial\xi_k}{\partial x_j}\frac{\partial u_i}{\partial\xi_k}$$

Where:

$$\tau_{ij}=\mu_t\left(\frac{\partial\xi_k}{\partial x_j}\frac{\partial u_i}{\partial\xi_k}+\frac{\partial\xi_k}{\partial x_i}\frac{\partial u_j}{\partial\xi_k}-\frac{2}{3}\delta_{ij}\frac{\partial\xi_l}{\partial x_k}\frac{\partial u_k}{\partial\xi_l}\right)$$

The Sutherland law is employed for the molecular viscosity coefficient μ. The turbulence eddy viscosity coefficient μ_t and other standard k-ε model constants are defined as:

$$\mu_t=C_\mu\rho\frac{k^2}{\varepsilon}$$

$$C_\mu = 0.009,\ C_{\varepsilon1} = 1.44,\ C_{\varepsilon2} = 1.92,\ \sigma_\varepsilon = 1.3$$

The upwind Van Leer's scheme based on flux vector splitting is implemented for the spatial discretization. By employing the Mid Mod limiter, the first-order Van Leer's scheme is extend to a second-order spatial accuracy. A central difference scheme is used to discretize the viscous diffusive terms. The explicit Runge-Kutta algorithm is employed for time integration.

The computation domain and grid distribution is shown in Fig. 2. The center of the spherical cap is the origin, the centerline of the reentry capsule is the axis, a two-dimensional axisymmetric computation domain is established. The distance from the left boundary, the right boundary and the upper boundary vertices to the origin is 7.5, 5.5 and 10 R, respectively. The grid topology is carefully designed to ensure the computation accuracy and the computation domain is divided into 12 sub-domains for constructing of structural grid. Considering the sharp variation of flow parameter in the shock layer and near wall grid requirement for heat flux

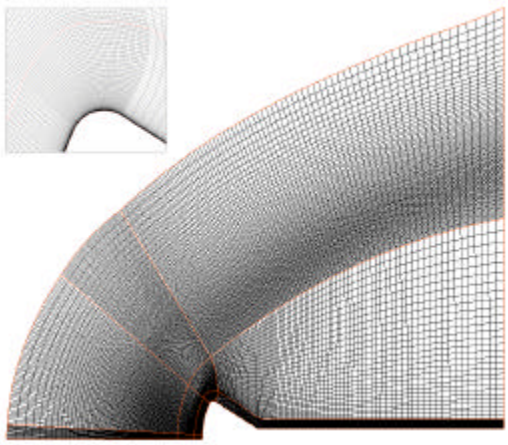

Fig. 2: Computation area and mesh distribution near the wall

computation, grid near the body surface is refined and a grid dependency test is taken which will be discussed in detail in the section of grid dependency test.

In the present study, the boundary conditions are given as follows. Because all cases are run at zero angle of attack and are forced to be symmetrical by imposing symmetry conditions along the centerline of the model. For the far field, the undisturbed free-stream condition at the upstream is specified as: $M_\infty = 3.48$, $U_\infty = 677$ m sec^{-1}, $V_\infty = 0$, P_∞=4201 Pa, $T_\infty = 94.2$ K. The outflow boundaries used simple extrapolation for all variables. Viscous, non-slip and constant temperature condition are applied on the body surface. At the jet exit, The jet total temperature is kept at 284.2 and Mach number is 2.94 for all cases while the jet total pressure is varied with the increasing of P from its minimum value of 1. If the poj is less than pof, there will be no outflow at the nozzle exit.

RESULTS AND DISCUSSION

Grid dependency test: The heat flux is very sensitive to the grid distribution near the wall surface has been the consensus of researchers and widely studied (Cockrell *et al*., 2002; Dilley, 2001; Hoffmann *et al*., 1991). In this study, for accurate aero-thermal environment simulation, four sets of grid listed in Table 1 are constructed based on the wall cell Reynolds number $Re_{cell} = \rho_\infty u_\infty \Delta n/\mu_\infty$, where Δn is the normal grid spacing at the wall. The physical free-stream parameter of $M_\infty = 12$, $U_\infty = 1832$, $V_\infty = 0$, $P_\infty = 128.42$, T_∞=57 K are used in this study. The heat flux and pressure distribution on the body surface are shown in Fig. 3 and are compared with experiment data (Matthew *et al*., 2008). The comparison shows the feature and trends in the experiment image to be captured well by the computational simulation. Because the Cell Reynolds number of Grid1 is too large, the calculated heat flux is a little higher than the experiment result. With the decreasing of normal grid spacing, the heat flux of Grid2 and Grid3 gradually close to the experiment result. However, further increasing the Cell Reynolds number, the heat flux of Grid4 doesn't show a better agreement with experiment data than Grid3. Considering the heat flux of Grid2, Grid3 and Grid4 agrees well with experiment data within 10% deviation which is generally within the experimental uncertainty, estimated to be around 15%, Grid3 type is used in this study. Generally, prediction of the aerodynamic environment only requires a low level of grid refinement (Hoffmann *et al*., 1991). The surface pressure distribution agree fairly well with the experiment results in all these four sets of grid type, so only the pressure distribution of Grid3 is given in Fig. 3.

Validation tests: To validate the numerical method, the supersonic flow field without counter-flow jet and with jet at the stagnation point are simulated and compared with experimental data. The non-dimensional bow shock

Table 1: Results of grid dependency study

Grid type	Grid distribution (angular×radial)	Δn	Re_{cell}	Heat flux rate at stagnation point (W m^{-2})
1	200×220	1.02E-4	308.00	35.23×10^4
2	200×220	1.02E-5	30.80	22.21×10^4
3	200×220	2.54E-6	7.72	20.48×10^4
4	200×220	1.05E-6	3.19	22.80×10^4

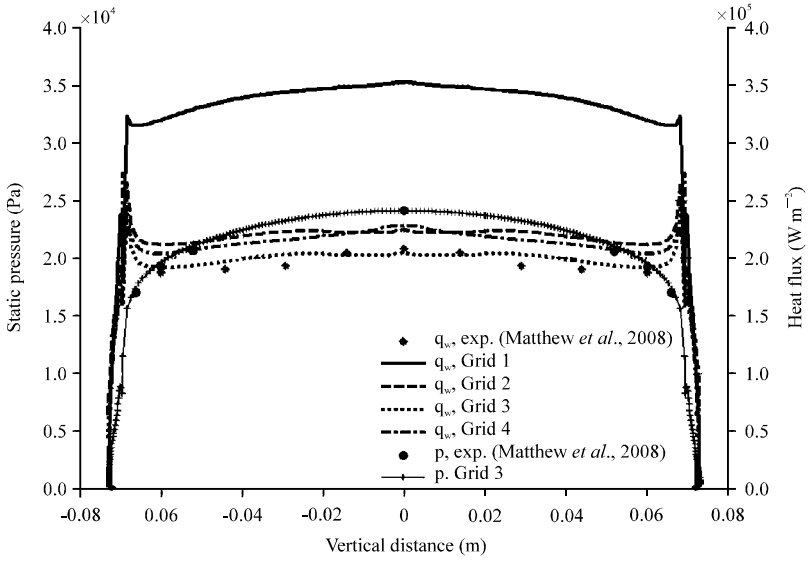

Fig. 3: Comparison of The heat flux and surface pressure distribution at different grid resolutions with experimental data

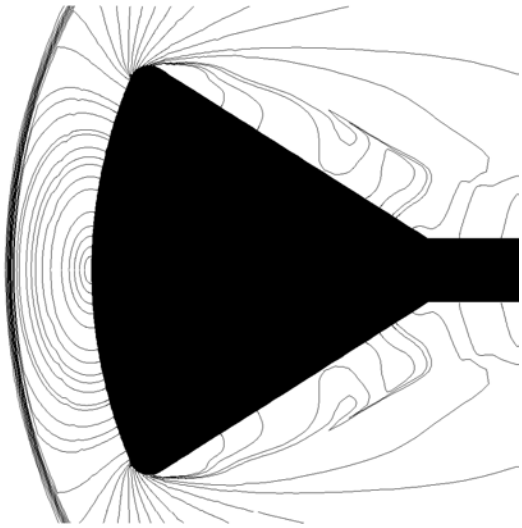

Fig. 4: The pressure contour with no jet at $Ma_\infty = 3.48$

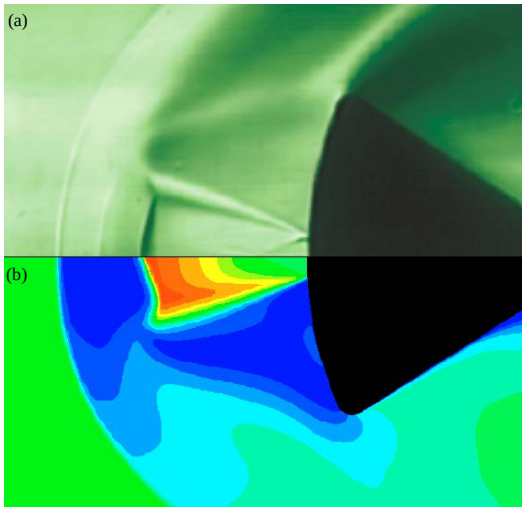

Fig. 5: The comparison of CFD results of pressure contour with schlieren data at P = 44.6, (a) Experiment results (Daso *et al*., 2009) and (b) The present computation

stand-off distance Δ/D of the flow without jet is 0.201 which agreed well with the experimental data (Daso *et al*., 2009) within 3% deviation. The pressure contour with no jet is shown in Fig. 4. For the convenience and direct of view, all the flow field contour in this paper is mirrored along the symmetry line. The mixing flow field structure with jet at P = 44.6 is also compared with experimental schlieren image in Fig. 5. This complex interacting flow field constitutes a new displacement shape with jet pushing the bow shock standing away from the body surface, there is Mach reflection at the jet exit and mach disk is shown. The fluid from the jet reverses its orientation as a conical free shear layer and is partly entrained to form a recirculation region. The conical shear layer triggers a series of compression wave because of reattachment to the body surface and a reattachment shock is then generated. The shock structure and flow field shape is consistent with the experiment schlieren image. All these agreement give us confidence on this numerical strategy.

Two flow modes: Numerical simulations under different jet total pressure ratio P of 1.8, 3.1, 4.5, 8.9, 16.0, 18.0, 22.3, 31.2, 44.6 are taken. With the jet Mach number and total temperature fixed, the other jet physical parameters shown in Table 2 can be obtained by employing local isentropic relations.

As the jet total pressure ratio of P increases from its minimum value of 1, the jet issuing from the stagnation point displace the bow shock upstream far away and reverse it orientation immediately downstream by the mach disk. The deviation of the jet back to the body surface results in a complicated conical shear layer. A part of the jet stream is entrained to form a recirculation zone beneath the free shear layer. As the free shear layer reattaches to the body surface, the flow realigns with the body contour and triggers a series of compression wave, a reattachment shock is then generated at the should of the reentry capsule which intersects downstream with the bow shock to form a triple point.

Two flow modes are identified with the variation of P. One is Long Penetration Mode (LPM) which occurred at low value of jet total pressure ratio of P which is found

Table 2: Jet flow condition for simulation

Mach No.	X velocity (m ses^{-1})	Y velocity (m sec^{-1})	Total temperature (K)	Jet total pressure ratio	Static pressure (Pa)	Density (kg m^{-3})	Mass flow rate (kg sec^{-1})
2.94	-601.5	0	284.2	1.8	3454	0.115	0.0090
				3.1	6263	0.209	0.0159
				4.5	8942	0.299	0.0227
				8.9	17884	0.598	0.0453
				16.0	32183	1.076	0.0817
				22.3	44710	1.495	0.1130
				31.2	62594	2.093	0.1580
				44.6	89420	2.990	0.2270

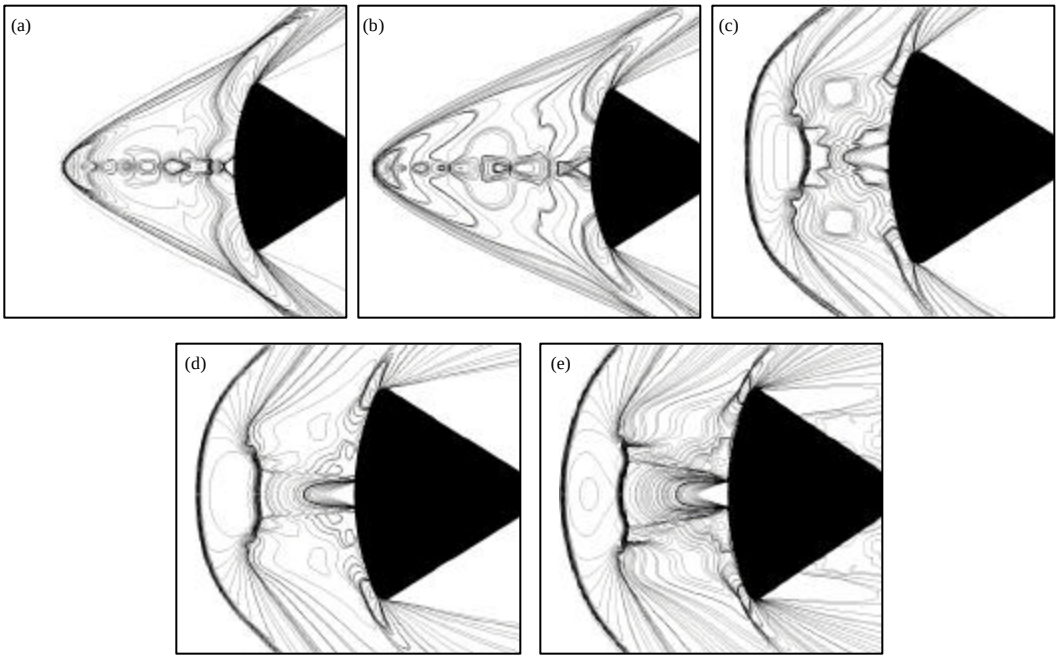

Fig. 6(a-e): Pressure contour of two flow mode with the variation of P, (a) P = 4.5, (b) P = 8.9, (c) P = 22.3, (d) P = 31.2 and (e) P = 44.6

to be unsteady shown in Fig. 6a and b at P = 4.5 and P = 8.9. The jet penetrates through with large shock stand-off distance, there is multiple-cell structure occur in the jet column, the modified shock envelop is generally conical. The other is Short Penetration Mode (SPM) which occurred at relative high value of P and both the drag force and shock-wave structure settle to a nearly steady state shown in Fig. 6c-e at P = 22.3, P = 31.2 and P = 44.6, respectively. The jet penetrate through with reduced standoff distance, the jet exhibits a single-cell structure with a well established Mach disk at the end of the jet column, the modified shock envelop resembled the blunt body. The flow transition from LPM to SPM is sudden at the critical value of $P_{crit} = 16.0$.

An important characteristic of the flow fields with LPM jet is the rather pronounced unsteadiness and oscillation. This periodic oscillatory motion in the long penetration mode at P = 3.1 is shown in Fig. 7a-e within one cycle. A definitive explanation for this self-sustaining unsteadiness and oscillation at low jet total pressure ratio has remained elusive due the complexity of this flow field. It maybe resulted from the pressure perturbation in the free shear layer which will propagate upstream to the mach disk though the subsonic recirculation zone due to adverse pressure gradient. However, when the counter-flow jet total pressure is high enough, the supersonic jet stream separates the subsonic recirculation domain and the subsonic region immediately downstream of the Mach disk to break down the propagation of pressure disturbance and the flow will returns to nearly steady motion.

The mode of flow motion depends upon the driving nozzle stagnation pressure and therefore the type of nozzle expansion type. That is, whether the jet was under-expanded, fully expanded, or over-expanded, based on the pressure difference between the nozzle exit static pressure and the static pressure of the ambient or shocked flow. Within the critical value of P the flow is in unsteady state. The jet flow is over or fully expanded which undergoes a series of expansion waves and then experiences a pair of oblique shocks in the plane to form an X-type structure as the small-scale vertical structures in the jet column shown in Fig. 6a and b. The flow is in LPM. Beyond the critical value of P there steady state mode as shown in Fig. 6c-e, the jet is under-expanded and the structure exhibits a Mach reflection with a well established Mach disk and barrel shock. A reflected shock is formed from the intersection of the barrel shock with the Mach disk.

Drag and heat flux reduction effect

Drag reduction: With the introducing of counter-flow jet, the main shock is pushed away from the body surface and strongly changed flow field and shock structure. The

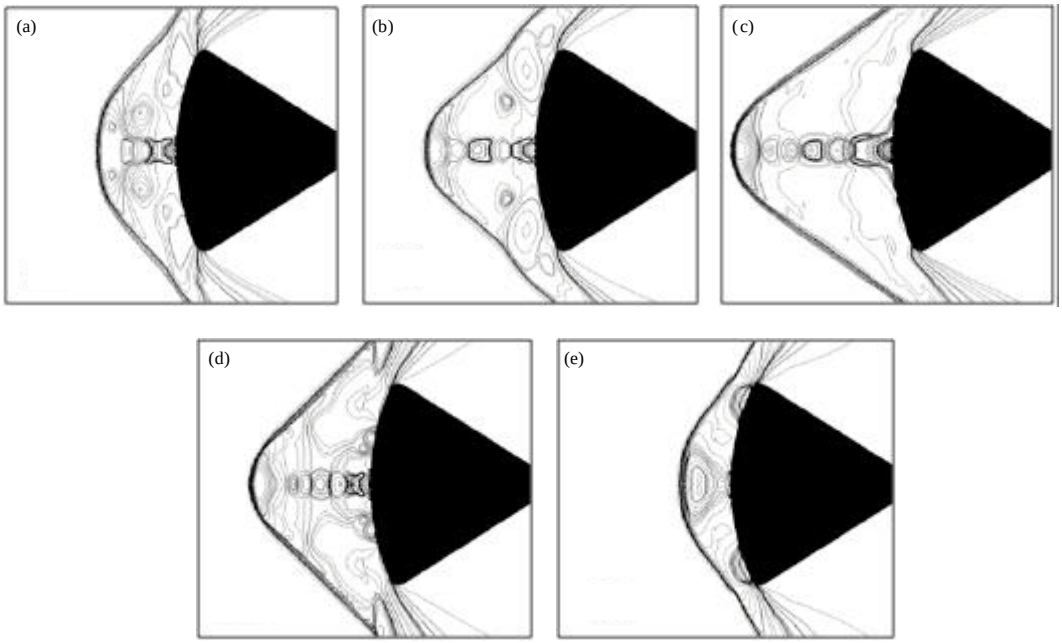

Fig. 7(a-e): Pressure contours in a cycle of unsteady LPM oscillatory motion at P = 3.1

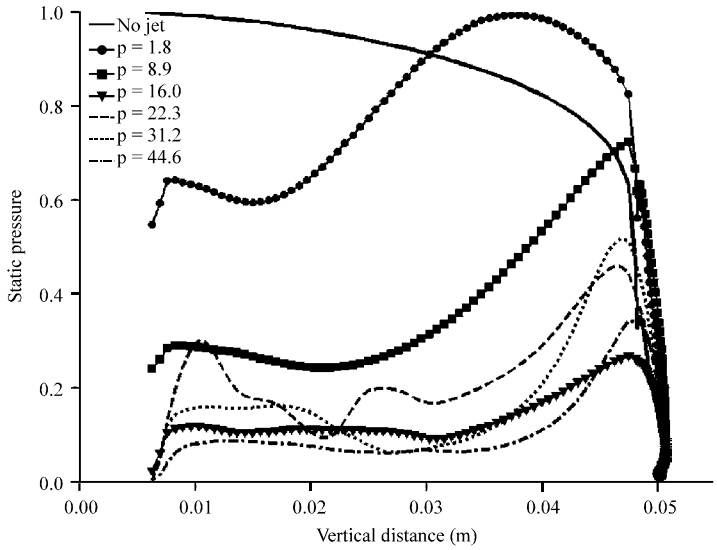

Fig. 8: Static pressure distribution on the body surface

time averaged non-dimensional static pressure p/p_{0f} distribution on the reentry capsule body surface under different P is given in Fig. 8. The no-injection curve is also shown for reference. The pressure on the body surface with counter-flow jet in the recirculation region is obviously much less than the stagnation-region pressures of the same body with no jet. With the increasing of P from 1, the general static pressure level on the body surface decline gradually until P_{crit} = 16.0 where the static pressure level reached a minimum value while as $P>P_{crit}$, it rise sharply and then sustains a gradually drop tendency with the increasing of P. This modified pressure distribution is consistently with the flow mode transition from LPM to SPM and cause the drag force change shown in Fig. 9.

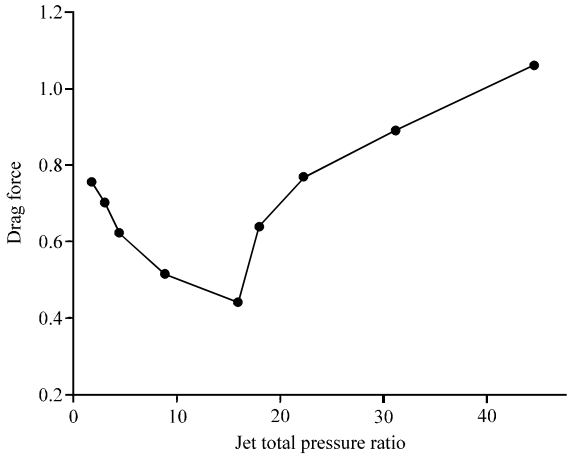

Fig. 9: The variation of drag coefficient to jet total pressure ratio P

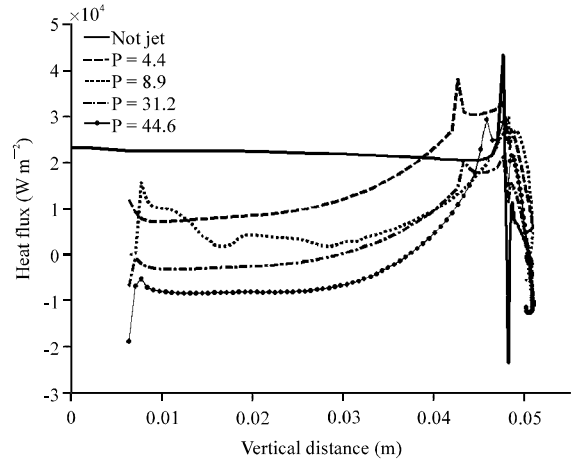

Fig. 10: Variation of body surface heat flux with jet total pressure ratio P

The non-dimensional drag force C_d/C_{d0} on the body surface variation with P is given in Fig. 9, where C_d is the body drag force with jet including the drag penalty of the counter-flow jet, C_{d0} for flow without jet. The exhausted thrust for producing of counter-flow jet:

$$T_j = mV_j + A_j p_j = A_j p_j(\gamma_j M_j^2 + 1)$$

is calculated, where V_j is the velocity at the jet exit, A_j is the area of jet exit. The drag on the body is reduced significantly because of counter-flow jet. With the increasing of P, the drag coefficient first fall continuously and after the injection pressure exceeds the critical value at $P_{crit} = 16.0$, the drag force increase sharply and sustains a continuously drop with a shallow slope. Because of the longer displacement of main shock pushed away from the body surface in LPM than in SPM, the drag reduction efficiency is better when flow is in LPM than in SPM. At P = 1.8, 3.1, 4.5, 8.9, 16.0, the drag is reduced by 24.5, 29.9, 37.7, 48.4 and 55.8%, respectively. As further increasing the jet total pressure ratio in SPM, the general static pressure level maybe lower than its counter-part in LPM as shown in Fig. 7, however, the net drag reduction efficiency are not shown to be increased. The upstream thrust created by the jet will contribute to the overall drag. There is a tradeoff between displacement of the main shock pushed away from body surface and the jet total pressure ratio. When P = 18.0, 22.3, 31.2, 44.6 at SPM, the drag is reduced by 36.2, 23.1, 11 and -5.9%, respectively. The maximum drag reduction condition is reached at $P_{crit} = 16.0$ in LPM.

Heat flux: Because the aero-thermal prediction is very sensitive to grid distribution, although the grid convergence tests have been taken, the change of jet flow mode with the increasing of P and the nature complexity of flow field may change the grid requirement, the heat flux variation in this paper will be only analyzed qualitatively. The heat flux distribution on the body surface under different jet total pressure ratio is shown in Fig. 10. Counter-flow jet greatly decreased the heat flux on the supersonic reentry capsule body. The heat flux decreased gradually with the increasing of P and even reached negative value in the recirculation region at high value of P = 31.2 and P = 44.6. However, the intersection and interference of the main shock and the reattachment shock at the capsule shoulder resulted in local high heat flux which maybe higher than their counterpart without jet.

CONCLUSIONS

A numerical simulation of a counter-flow jet issuing from the stagnation point of a reentry capsule body in supersonic flow is carried out. The flow motion mode and the effect of jet total pressure ratio on the drag and heat reduction efficiency is summarized as follows:

- With the increasing of P, the flow experience two flow modes: the former is long penetration mode, the latter is short penetration mode. The transition from LPM to SPM is sudden at P_{crit}. The jet penetrates through with large shock stand-off distance, there is multiple-cell structure occur in the jet column, the modified shock envelop is generally conical in LPM while the jet penetrate through with reduced standoff distance, the jet exhibits a single-cell structure with a well established Mach disk at the end of the jet column, the modified shock envelop resembled the blunt body in SPM

- With the introducing of counter-flow jet , the main shock is significantly pushed far away from the body surface, the general static pressure level on the body surface reduced obviously and resulted in the drag reduction. The drag reduction efficiency rises monotonically with the increasing of P except in the critical value of P where drag force rise sharply to form a discontinuity point. This is corresponding to the flow mode transition from LPM to SPM. The maximum drag reduction is obtained at P_{crit} at LPM which is as high as 55.8% for cases in this study
- The heat flux decreased gradually with the increasing of P and even reached negative value in the recirculation region at high value of P. However, the intersection and interference of the main shock and the reattachment shock at the capsule shoulder resulted in local high heat flux which maybe higher than their counterpart without jet.

ACKNOWLEDGMENT

This Project was supported by the State Key Program of National Natural Science of China (Grant No. 90715013).

REFERENCES

Chen, L.W., G.L. Wang and X.Y. Lu, 2011. Numerical investigation of a jet from a blunt body opposing a supersonic flow. J. Fluid Mech., 684: 85-110.

Cockrell, C.E. Jr., A.H. Auslender, J.A. White and A.D. Dilley, 2002. Aeroheating predictions for the X-43 hyper-X cowl-closed configuration at Mach 7 and 10. AIAA Paper 2002-02l8. http://ntrs.nasa.gov/archive/nasa/casi.ntrs.nasa.gov/20020016022_2002010072.pdf

Daso, E.O., V. Pritchett and T.S. Wang, 2009. Dynamics of shock dispersion and interactions in supersonic free-streams with counter-flowing jet. AIAA J., 47: 1313-1326.

Debieve, J.F., J.P. Ardissone and J.P. Dussauge, 2003. Shock motion and state of turbulence in a perturbed supersonic flow around a sphere. J. Turbul., 4: 1-15.

Dilley, A.D., 2001. Evaluation of CFD turbulent heating prediction techniques and comparison with hypersonic experimental data. NASA-CR-2001-210837. http://lsr.larc.nasa.gov/bitstream/2002/13644/1/NASA-2001-cr210837.pdf

Finley, P.J., 1966. The Flow of a jet from a body opposing a supersonic free stream. J. Fluid Mech., 26: 337-368.

Fomin, V.M., A.A. Maslov, A.P. Shashkin, T.A. Korotaeva and N.D. Malmuth, 2001. Flow regimes formed by a counter-flow jet in a supersonic flow. J. Appl. Mech. Tech. Phys., 42: 757-764.

Formin, V.M., A.A. Maslov, N.D. Malmuth, V.P. Fomichev and A.P. Shashkin *et al*., 2002. Influence of a counterflow plasma jet on supersonic blunt-body pressures. AIAA J., 40: 1170-1177.

Ganiev, Y.C., V.P. Gardeev, A.V. Krasilinikov, V.I. Lagutin, V.N. Otmenhikov and A.V. Panasenko, 2000. Aerodynamic drag reduction by plasma and hot-Gas injection. J. Thermophys. Heat Tr., 14: 10-17.

Hoffmann, K.A., M.S. Siddiqui and S.T. Chiang, 1991. Difficulties associated with the heat flux computations of high speed flows by the Navier-Stokes equation. AIAA Paper 1991-467.

Launder, B.E. and D.B. Spalding, 1974. The numerical computation of turbulent flows. Comp. Meth. Appl. Mech. Eng., 3: 269-289.

Matthew, M., M. Erik, W. Timothy, H. Michael and P. Ronald, 2008. Analysis and ground test of aerothermal effects on spherical capsule geometries. AIAA Paper 2008-4273. http://aric.inha.ac.kr/treatise/journal/content.asp?idx=107451&Search=Michael%20Holden&Select_field=Author&SearchVal=Michael%20Holden&SearchCheck=&page=1

Meyer, B., H.F. Nelson and D.W. Riggins, 2001. Hypersonic drag and heat transfer reduction using a forward-facing jet. J. Aircraft, 38: 680-686.

Nair, P., T. Jayachandran, M. Deepu, B.P. Puranik and U.V. Bhandarkar, 2010. Numerical simulation of interaction of sonic jet with high speed flow over a blunt body using solution mapped higher order accurate AUSM+-UP based flow solver. J. Appl. Fluid Mech., 3: 15-23.

Romeo, D.J. and J.R. Sterrett, 1963. Exploratory investigation of the effect of a forward-facing jet on the bow shock a blunt body in a Mach 6 Free Stream. NASA -TN-D-1605.

Shang, J.S., J. Hayes, K. Wurtzler and W. Strang, 2001. Jet spike bifurcation in high speed flows. AIAA J., 39: 1159-1165.

Shang, J.S., J. Haes and J. Menart, 2002. Hypersonic flow over a blunt body with plasma injection. J. Spacecraft Rocket, 39: 367-375.

Venukumar, B., G. Jagadeesh and K.P.J. Reddy, 2006. Counterflow drag reduction by supersonic jet for a blunt body in hypersonic flow. Phys. Fluids, 18: 81041-81044.

Warren, C.H.E., 1960. An experimental investigation of the effect of ejecting a coolant gas at the nose of a bluff body. J. Fluid Mech., 8: 400-417.